Study of reflection and transmission spectra of arrays of heterogeneous ferromagnetic nanowires in the terahertz and far infrared ranges

© L.A. Fomin,[1] D.L. Zagorskiy,[2] S.G. Chigarev,[3] E.A. Vilkov,[3] V.G. Krishtop,[1] I.M. Doludenko,[2] S.S. Zhukov[4]

[1] Institute of Microelectronic Technology and High-Purity Materials, Russian Academy of Sciences
142432 Chernogolovka, Moscow region, Russia
[2] Federal Research Center „Crystallography and Photonics" Russian Academy of Sciences,
119333 Moscow, Russia
[3] Fryazino branch of Kotelnikov Institute of Radio Engineering and Electronics RAS,
141190 Fryazino, Moscow region, Russia
[4] Moscow Institute of Physics and Technology (State University),
141700 Dolgoprudnyi, Moscow region, Russia
e-mail: fomin@iptm.ru

In the frequency range from 16 to 50 THz, the transmission, reflection, and absorption spectra of arrays of heterogeneous Ni/Co, FeNi/Co, and Ni/Fe nanowires grown in track polymer membranes by the galvanic method have been studied. The absorption spectra showed that the fraction of the radiation power absorbed by the nanowires and its spectrum depend on the materials of the nanowires. The features of the spectra can be explained by the accumulation of nonequilibrium spin due to electron diffusion and its relaxation stimulated by external terahertz (THz) radiation, which can be used to create a THz radiation detector. In addition, negative absorption was found for FeNi/Co nanowires, which can be explained by the laser effect on spin-flip transitions, which can be used to create a THz radiation source operating at room temperature.

Keywords: nanowires, THz radiation, THz spectroscopy, spin-flip transitions, metamaterial.

Introduction

In the last decade, interest in the terahertz (THz) frequency range has increased $(1-30$ THz). Radiation in this frequency range is used to solve problems of medicine and biology [1–3], astrophysics [4,5] and chemical research [6], security systems [7,8], as well as for telecommunication systems [9], in particular, for the implementation of universal and stable 6G/7G ultra-broadband communication networks in the future. Sources of THz radiation, even with low intensity, may be of interest for quantum cryptography problems. In protocols with continuous variable quantum key distribution (CV-QKD), instead of purely Gaussian states, „noisy" coherent states, the so-called „thermal states" [10], can be used. The quantum distribution of keys over thermal states can work in the infrared (IR) range up to units of terahertz [11], which may be interesting for „last mile" [12] or satellite communications [13].

However, the successful study of the THz band and the development of THz technology is hindered by the lack of simple and reliable publicly available sources and receivers of such radiation. The commercially available sources of THz radiation available today, such as reverse wave lamps, free electron lasers, gas lasers and gas-discharge sources of THz radiation, are far from meeting the requirements of simplicity and reliability. Similarly, the development of new receivers of THz signals is required, since currently quite

inertial Golay cells are used, as well as superconducting bolometers operating at low temperatures and requiring cryogenic equipment.

Thus, the task of finding new principles for the formation and registration of THz signals is extremely urgent. One of the promising directions for the development of THz electronics is the development of generators and detectors of THz-signals based on the principles of spintronics using magnetic transitions in nanostructures. So, in particular, certain successes have been achieved in the development of THz generators operating on the basis of injection of spin-polarized current in magnetic transitions, the possibility of creating which was predicted in theoretical works [14–16] and experimentally confirmed in the studies [17,18]. An important feature of such systems is their high performance and reliable operation in a wide temperature range, including at room temperatures.

To date, a number of spin-injection sources of THz radiation have been developed and experimentally investigated using various structures of magnetic transitions [19–22], however, no attempts have been made to create THz detectors operating on these principles.

From the point of view of miniaturization and at the same time increasing the efficiency of radiation reception, the use of metamaterials for detecting the THz signal is of interest. One of such metamaterials may be a lattice of conducting parallel thin wires [23], which has quite

Electrolytes and modes

№	Deposited Metal	Metal salt	Concentration, g/l	Additives	Deposition potential, V
1	Fe	$FeSO_4 \cdot 7H_2O$	120	Boric acid (40 g/l); Sodium Lauryl Sulfate (0.5 g/l); Ascorbic acid (1 g/l)	1
2	Ni	$NiSO_4 \cdot 7H_2O$ $NiCl_2 \cdot 6H_2O$	200 30	Boric acid (40 g/l); Sodium Lauryl Sulfate (1 g/l)	1.2
3	Co	$CoSO_4 \cdot 7H_2O$	320	Boric acid(40 g/l); Sodium Lauryl Sulfate (1 g/l)	0.8
4	FeNi	$FeSO_4 \cdot 7H_2O$ $NiSO_4 \cdot 7H_2O$ $NiCl_2 \cdot 6H_2O$	8 16 40	Boric acid (25 g/l); Sodium Lauryl Sulfate (0.5 g/l); Ascorbic acid (1 g/l)	1.5

interesting optical properties. Thus, in the study [24], an experimental demonstration of an ultra-high-resolution image was presented using a three-dimensional nanolens consisting of parallel gold nanowires (NW) embedded in a porous aluminum oxide matrix. The principle of focusing radiation using such metamaterials can also be applied to THz frequencies, in particular, in the study [25] visualization in THz was demonstrated with unprecedented propagation of near-field information over hundreds of wavelengths and focusing up to 1/28 wavelength. In the study [26], a theoretical study of the magneto-optical properties of cylindrical metallic NW was carried out. It has been shown that the resonant absorption frequencies of these wires are in the THz range and can be effectively tuned by changing the radius of NW, as well as by applying an external magnetic field.

Thus, it is of interest to study the optical properties of metamaterials from magnetic metallic NW, in particular, heterogeneous ones, in which the injection of spin-polarized current from one material into another is possible.

From the point of view of manufacturing metal NW arrays, the method of electrochemical deposition into the pores of track membranes [27,28] is of interest. These membranes are relatively easy to manufacture, and this technology allows for extensive experimentation with various materials and their combinations.

In this paper, the reflection and transmission spectra of structures based on an array of heterogeneous NW were studied. Three types of samples with ferromagnetic transitions formed between alternating layers of Ni/Co, FeNi/Co and Ni/Fe were studied.

1. Sample preparation

Arrays of heterogeneous NW from Ni/Co, Fe Ni/Co and Ni/Fe were manufactured by matrix synthesis using track membranes manufactured by JINR (Joint Institute for Nuclear Research, Dubna city) as matrices. The membranes were porous films of polyethylene terephthalate with a thickness of 12μm with a pore diameter of 100 nm and a pore density of $1.2 \cdot 10^9 \, cm^{-2}$. NW were synthesized by electroplating by filling the pores with metals from a solution of the corresponding salts. Electrolytes, stabilizing additives and deposition modes for each deposited metal (or alloy) are presented in the following table.

The preparation of heterostructural NW took place in several stages. At the first stage, a solid copper layer with a thickness of 4, μm was applied on one side of the matrix, which played the role of contact during electrodeposition. Further, electrochemical deposition of metals was carried out in the pores of the matrix. It is worth noting that the process was carried out in a potentiostatic mode using an anode corresponding to the deposited metal, and an iron anode was used during the deposition of FeNi. Deposition potentials are shown in the table. The deposition process was controlled by the leaking charge. This method made it possible to control the length more precisely and gave high reproducibility of the results.

In this study, samples with NW consisting of two or three layers of different metals (and respectively with one or two contacts-heterojunctions between them) were synthesized. At the stage of galvanic pore filling, the growth of NW from alternating layers of metals was carried out by changing the corresponding electrolytes in the cell. At each shift, before moving to the filling stage with another metal, distilled water was washed. At the last stage of galvanic deposition, a copper electrolyte was used — the pores were filled with copper „to the end ", subsequent growth led to the formation of a solid layer of copper on the surface of the growth matrix.

The goal of the next stage was to create a network of conductive strips on both sides of the membrane. For this purpose, lithography methods were used: thin films were applied to both copper-metallized surfaces of the membrane with NW $(0.7-1$ mm) parallel strips of „protective" material (resist, permanent marker). The gaps between the strips were also about 1 mm. Note that the stripes on both sides of the matrix were applied perpendicular to each other. Subsequent dissolution of copper (in ammonium hydroxide solution) led to local etching of unprotected areas. The
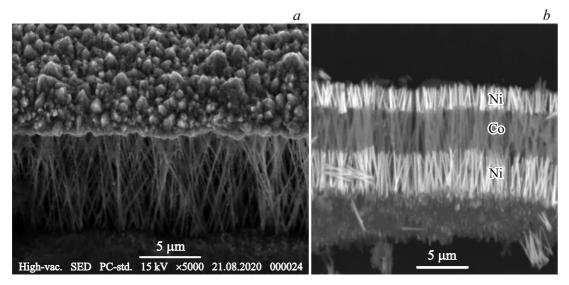
Figure 1. SEM image of the NW array (*a*) and the NW contrast itself from different materials (*b*).

result of the process was the creation of parallel copper strips on the surfaces of the system, alternating with „open" areas. Such a scheme provided partial transparency of the sample — radiation could pass through „open" (non-metallized) regions. At the same time, the contact strips provided a current supply to a part of the NW (enclosed between the strips) in the matrix. The nature of the arrangement of the strips — perpendicular direction on opposite sides of the sample — provided an increase in effective electrical resistance due to the serial connection of the NW beams located between the copper strips into the chain.

The manufactured samples were examined by scanning electron microscopy (SEM) with elemental analysis using a JEOL JSM 6000 Plus device with an accelerating voltage of 15 kV. The resulting images of NW arrays are shown in Fig. 1.

The figure shows that almost all the pores of the membranes are filled with metal (Fig. 1, *a*), and clear boundaries are observed between different metals in all NW (Fig. 1, *b*).

Schematic representation of contact strips with NW between them is shown in Fig. 2, *a*, and SEM image of the contact strip system (after removal of the polymer matrix) is shown in Fig. 2, *b*.

2. Spectral analysis

The synthesized samples (arrays of NW with heterojunctions and contact bands on the matrix surface) were studied by spectral analysis methods. Reflection and transmission spectra were obtained.

The spectra were measured using a Bruker Vertex 80v IR Fourier spectrometer with a Hyperion 2000 microscope in the air in the range of 15−250 THz. The diagram of

the experimental bench is presented in Fig. 3. In these experiments, the spectrum of the signals reflected from the NW membrane and transmitted through it was measured. During measurements, the thermal source of THz radiation MIR (Medium InfraRed), — globar was located in the spectrometer housing. The broadband radiation of the globar was fed into a high-quality open resonator, tunable in frequency. This made it possible to have a frequency-tunable signal at the output of the spectrometer, which went through the block of light filters to the output OUT 1, and from it — into the microscope. There he was directed in one direction or another by a movable mirror.

Thus, at the position of the mirror shown in Fig. 3, the beam of radiation from the globar was focused using a microscope on the area of the sample with NW, not closed by contact strips. The signal passed through the sample in this way was recorded by a nitrogen-cooled MCT detector (Mercury Cadmium Telluride) installed in the Hyperion microscope. The spectrum of the transmitted signal was measured in this way. To measure the spectrum of the reflected signal, the mirror was rotated, and the beam, passing through the lens, fell on the sample. The radiation reflected from the surface of the sample fell on the detector. Since the NW length was $12 \mu m$, their diameter — 100 nm and the distances between them were estimated as tens of nanometers, for the wavelengths of the studied spectrum (ten or more microns), the NW array can be considered as a metamaterial. The incident signal is divided into reflected, transmitted and absorbed, the total intensity of which is equal to the intensity of the incident signal.

The influence of the materials of the NW layers on the spectral characteristics was studied. The results obtained are presented in Fig. 4: spectra of R reflected (*a*) and T transmitted (*b*) signals for NW with transitions NiFe/Co, Ni/Co and Ni/Fe. Note that the results obtained were adjusted
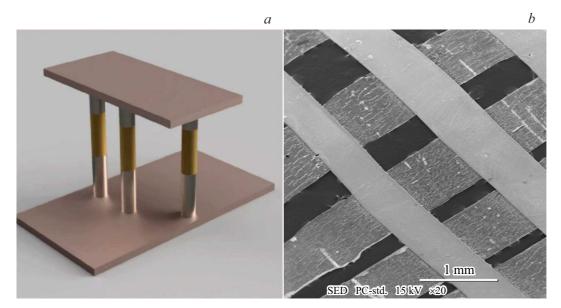
Figure 2. Schematic representation of NW (with three layers of different metals) between the contact strips (*a*); SEM image of the contact strip system (on two sides of the original matrix; in the image, the matrix is removed) (*b*).
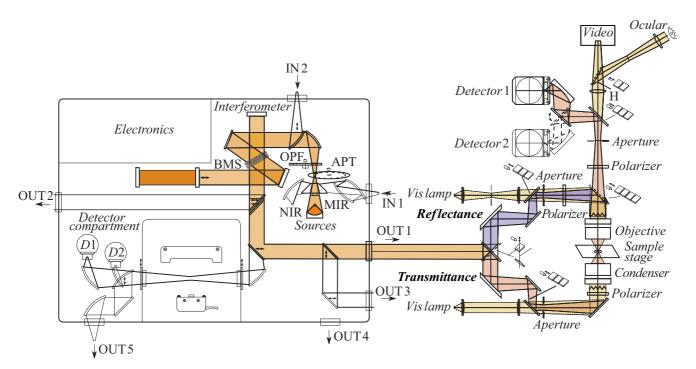

Figure 3. Diagram of the experimental unit. On the left is a diagram of the Bruker Vertex V80 IR-Fourier spectrometer, on the right is a diagram of the Hyperion 2000 IR-Fourier microscope connected to it. Orange stripe (in online version) — the optical path from the THz radiation source of the globar embedded in the spectrometer (MIR) through the Sample Stage to the *D*1 or *D*2 detectors installed in the microscope. A part of the optical path is highlighted in blue (in the online version) when measuring the spectrum of the reflected signal.

for changes in measurement conditions, for changes in the globar spectrum and for the influence of the polymer matrix (see below). To correct the change in the characteristics of the device during measurements, with each measurement of the spectrum of radiation transmitted through the sample, the spectrum of radiation transmitted along the same optical path, but without the sample, was then also measured. Then the spectrum of radiation transmitted through the sample was divided into the spectrum of radiation transmitted in the absence of the sample. Similarly, when measuring the spectra of radiation reflected from the sample, these spectra were divided into the spectrum of reflection from the reference gold mirror, which was installed in place of the sample.
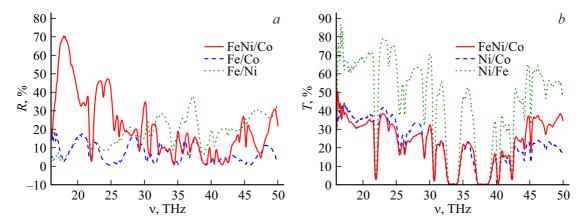
Figure 4. Reflection spectra (*a*) and transmission (*b*) of NW arrays with NiFe/Cu, Ni/Co and Ni/Fe transitions, (correction — division by the globar radiation spectrum).
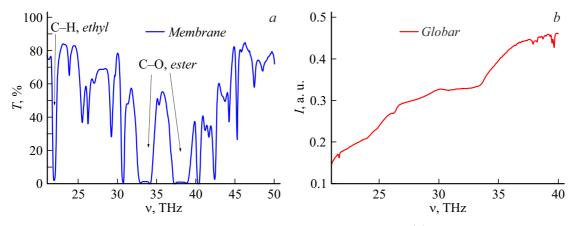

Figure 5. The transmission spectrum of a porous membrane divided by the globar spectrum (*a*). For comparison, the spectrum of globar radiation (*b*) is given.

As can be seen from Fig. 4, the reflectivity of the surface depends on the materials of the NW, which leads to the appearance of a large number of characteristic lines even in that range (16−40 THz), where the globar spectrum is relatively monotone (Fig. 5, *b*). The monotony of the source spectrum excludes the formation of parasitic peaks in the spectra of samples as a result of division into this spectrum, which could be formed if the source spectrum had minima close to zero.

To account for the influence of the polymer matrix, the transmission spectrum of the membrane without NW was obtained (Fig. 5, *a*). As can be seen from the figure, most of the radiation passes through the membrane. The transmission spectrum of the membrane is not monotonous enough, and has absorption bands that correspond to fluctuations of different chemical groups. The strongest absorption is given by the ethereal C−O-groups. In general, the spectrum practically coincides with the known transmission spectrum of the membrane material (polyethylene terephthalate) [29].

A comparison of the spectra shown in Fig. 4, *b* and *a* shows that NW significantly affect the spectrum of the signal transmitted through the membrane. To more clearly

identify this effect, it is necessary to remove the growth polymer membrane — the authors suggest doing this in further studies.

The absorption spectra of a membrane with NW, determined by subtracting the sum of the transmission and reflection spectra from the radiation spectrum of the globar, are shown in Fig. 6.

The analysis of the spectra shows that, despite the similarity in the positions of the peaks for different NW, there are differences in the magnitude of these peaks. These features are related to the difference in materials NW. The sample with Fe/Co NW absorbs the most (50−80% from the intensity of the source), less absorption is observed in Fe Ni/Co NW and even less in samples Fe/Ni. At the same time, the latter wire material has the highest and sharpest absorption peaks (10−90% from the intensity of the source). An interesting result was obtained for Fe Ni/Co wires: in the range of 17−19 THz, negative absorption is observed for them.

It is known that the sum of the signals (transmitted, reflected and absorbed) must be equal to the power of the incident radiation for all frequencies of the spectrum.
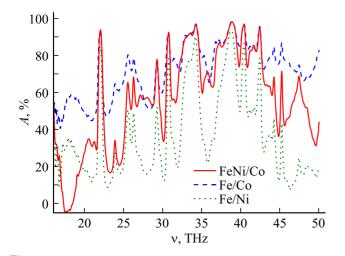
Figure 6. Absorption spectra of samples divided by the emission spectrum of the globar.

However, in the case when the sample is an optically active medium, it is possible to redistribute (transfer) power over frequencies so that a violation of this equality is observed in some frequency ranges. At the same time, the sample itself emits at certain frequencies, and the absorption on them becomes negative. The obtained result suggests that this sample may be optically active in the specified frequency range.

3. Theoretical discussion

We believe that in the studied metamaterials, it is possible to implement the mechanism of the reverse laser effect in the THz range based on spin-flip transitions [15,16], which can be used to create a THz radiation detector operating at room temperature. However, with homogeneous magnetization of the ferromagnetic medium, the matrix element for the spin-flip transition operator turns out to be zero [30]. Therefore, to implement the mentioned mechanism of interaction of electrons with THz radiation, either the exchange interaction constant must be a tensor in spin indices [30], or the magnetization of the medium must be heterogeneous [31]. In the second case, the spin parts of the wave functions of the conduction electrons have a more complex form than with homogeneous magnetization of the medium, which leads to the fact that the matrix element of the spin-flip transition is not zero. Thus, generation and absorption of THz radiation at the spin-flip junction is possible. To test this hypothesis, it is of interest to study the magnetic structure of NW.
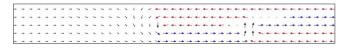

Figure 7. Magnetic structure of Co/NiFe wires calculated by the micromagnetism method.

The magnetic structure of the wires was calculated by the micromagnetism method using the OOMMF [32] program. NW in calculations was a cylinder with a length of $10\,\mu$m and a diameter of $100\,$nm. It was divided into cubic cells of the account with the edge of the cube $10\,$nm. For half the length of the cylinder, the magnetic parameters of one material were set, for the second half — of the other. The initial magnetization distribution was set randomly. The calculation result for Co/NiFe wires is shown in Fig. 7. It can be seen that near the boundary of the two materials, the magnetic structure is heterogeneous.

To begin with, let's consider the mechanism of generating THz radiation on a spin-flip transition. Since there is an heterogeneous magnetization distribution at the boundary of two metals for a system of bound electrons, it will lead to the fact that when a spin-polarized current is passed from one metal (injector) to another (working area) through this boundary, the spins of the injected electrons are not parallel to the magnetization in the working area where they fall, which stimulates radiative transitions electrons from the upper spin subband to the lower one.

For certainty, consider the magnetic transition nickel−iron (Fig. 8). Nickel has much more electrons with spin down at the Fermi level than up, since the d band for electrons with spin up is completely below the Fermi level in energy, and for electrons with spin down, the Fermi level almost coincides with the maximum density of states. In iron, the concentrations of electrons with both spin projections at the Fermi level are approximately equal. When materials come into contact, the diffusion of electrons from one to the other takes place. Let's assume for a start that spin does not relax (although, of course, there are relaxation channels by absorbing phonons or magnons, but we will neglect them for now). Then excess electrons will accumulate in the iron with a spin down, and the distribution of electrons will become nonequilibrium. Nonequilibrium electrons have corresponding nonequilibrium quasi-Fermi levels ε_{F+} and ε_{F-}, counted from the bottom of the lower spin subband. Under nonequilibrium conditions, radiative electronic transitions are possible from occupied states located below the quasi-Fermi level ε_{F+} for the minor spin subband to free electronic states located above the quasi-Fermi level ε_{F-} for the major spin subband. In order for the system to remain nonequilibrium, it is necessary that a voltage of V be applied to it. If the quasi-Fermi level ε_{F+} is shifted relative to the equilibrium value of the Fermi level of the working area by $\Delta\varepsilon_{F+} = \varepsilon_{F+} - (\varepsilon_{F0+} - eV/2)$, and the quasi-Fermi level ε_F by the value of $\Delta\varepsilon_{F-} = (\varepsilon_{F0-} - eV/2) - \varepsilon_{F-}$, then the maximum radiation frequency can also be represented as the sum of the values of $\Delta\varepsilon_{F+}$ and $\Delta\varepsilon_{F-}$ divided by Planck's constant:

$$\nu \equiv \frac{\Delta\varepsilon_{F+} + \Delta\varepsilon_{F-}}{2\pi\hbar} = \frac{|\varepsilon_{F+} - \varepsilon_{F0+}| + |\varepsilon_{F-} - \varepsilon_{F0-}|}{2\pi\hbar}. \quad (1)$$

We have introduced the signs of the module here so that this formula corresponds to any sign of ΔP. In general, the maximum frequency may correspond to an indirect
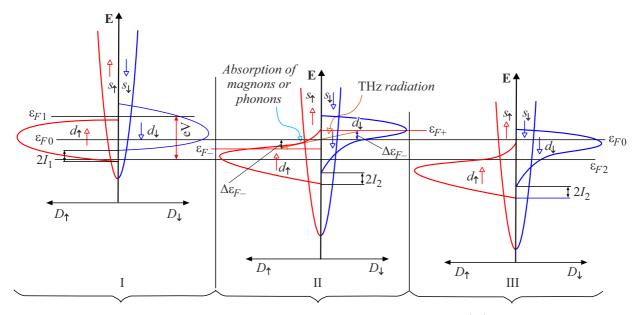
Figure 8. Diagram of energy electronic zones and quasi-Fermi levels: I — in the first ferromagnet (Ni), II — for nonequilibrium electrons in the second ferromagnet (Fe), III — for equilibrium electrons in the second ferromagnet.

radiative transition (with the participation of a third particle, for example, phonon, magnon, etc.). Formula (1) is written under the condition that the frequency of the third particle is negligible. In the general case, in this expression, from ν it is necessary to subtract the frequency of the third particle, $\nu_{F,m}$, since part of the energy is spent on the birth of the third particle. Note also that if $\Delta\varepsilon_{F+} + \Delta\varepsilon_{F-} \geq 2I_2$, then direct radiative transitions are also possible.

The values of the quasi-levels of the subbands depend on the nonequilibrium spin polarization and energy exchange splitting (I_2):

$$\varepsilon_{F+} = \frac{\hbar^2}{2m} (3\pi^2 n)^{2/3} \left[\left(\frac{1 - P_2 + |\Delta P|}{2} \right)^{2/3} \right] + 2I_2, \quad (2a)$$

$$\varepsilon_{F-} = \frac{\hbar^2}{2m} (3\pi^2 n)^{2/3} \left[\left(\frac{1 + P_2 - |\Delta P|}{2} \right)^{2/3} \right], \quad (2b)$$

where the assumption was used that one electron has a phase volume of $(2\pi\hbar)^3$ and the number of electrons with one direction of spin $n_{-,+} = n(1 \pm P)/2$ is equal to the volume divided by $(2\pi\hbar)^3$ spheres with a radius equal to the Fermi momentum.

Further, it is more convenient to express the change of quasi-levels in terms of the equilibrium value (P_2) and the nonequilibrium addition (ΔP) as follows:

$$\varepsilon_{F+} - \varepsilon_{0F+} = \frac{\hbar^2}{2m} (3\pi^2 n)^{2/3} \left(\left(\frac{1 - P_2 - \Delta P}{2} \right)^{2/3} \right.$$
$$\left. - \left(\frac{1 - P_2}{2} \right)^{2/3} \right), \quad (3a)$$

$$\varepsilon_{F-} - \varepsilon_{0F-} = \frac{\hbar^2}{2m} (3\pi^2 n)^{2/3} \left(\left(\frac{1 + P_2}{2} \right)^{2/3} \right.$$
$$\left. - \left(\frac{1 + P_2 + \Delta P}{2} \right)^{2/3} \right). \quad (3b)$$

In the formulas (3a) and (3b), the sign of the quasi-level changes depends on the sign of the nonequilibrium spin additive and can be either positive or negative. For this reason, in the formula (1) a modulus sign was introduced for the radiation frequency so that they correspond to any sign of ΔP.

Calculate the frequency for the Ni/Fe transition. The equilibrium spin polarization of Ni is 0.6, iron — 0.4. Thus, the maximum nonequilibrium addition of ΔP to the polarization for each of the metals is approximately 0.2. The maximum frequency calculated by the eq. (1) corresponding to this nonequilibrium additive is 20 THz. In the experiment, the maximum luminescence occurs at a frequency of 14 THz. From eq. (1) it follows that the nonequilibrium additive ΔP in this case is close to the maximum and is equal to 0.15.

Now we can consider the absorption of THz radiation. In this case, the opposite effect is possible with respect to the generation of radiation, which can be formulated as follows. The presence of external radiation activates the spin relaxation mechanism, and an absorption peak occurs at the frequency corresponding to the difference of the quasi-Fermi levels. At the same time, due to the accumulation of charge due to the diffusion of electrons, a voltage arises at the external contacts of the sample. By measuring this voltage, THz radiation can be detected.

Thus, the differences found in the magnitude of absorption peaks and other features in the spectra characteristic

of specific NW materials can be explained by the reverse laser effect on spin-flip transitions in the presence of THz radiation. A direct laser effect is also possible when pumping at higher frequencies, which can explain the negative absorption for FeNi/Co wires. The magnetic structure of the wires is mostly uniform except for the area of their contact.

Conclusion

Transmission and reflection spectra of two-component NW made of ferromagnetic metals in a polymer membrane in the frequency range $16-50$ THz are investigated. On the basis of experimental data, their absorption spectra were calculated, in which it was found that the amplitude and position of the spectral lines depend on the combination of metals in NW.

The features in the observed spectra can be explained by the accumulation of nonequilibrium spin due to electron diffusion across the boundary between two different ferromagnetic metals and spin relaxation stimulated by external THz radiation. In this case, a voltage should occur at the external contacts of the sample, which allows detecting THz radiation.

In addition, for NW from FeNi/Co: in $17-19$ THz negative absorption was detected, which can be explained by the laser effect on spin-flip transitions when pumped at higher frequencies, which can be used to create a source of THz radiation.

Conflict of interest

The authors declare that they have no conflict of interest.

References

[1] S. Wang, X.-C. Zhang. J. Phys. D: Appl. Phys., **37**, R1 (2004). DOI: 10.1088/0022-3727/37/4/R01

[2] Q. Sun, Y. He, K. Liu, S. Fan, E.P.J. Parrott, E. Pickwell-MacPherson. Quant Imaging Med. Surg., **7** (3), 345 (2017). DOI: 10.21037/qims.2017.06.02

[3] P. Siegel. IEEE Trans. On Microwave Techniq., **52** (10), 2438 (2004). DOI: 10.1109/TMTT.2004.835916

[4] S. Molinari, A. Noriega-Crespo. Astronomical J., **123**, 2010 (2002). DOI: 10.1086/339180

[5] L.L. Leeuw, T.G. Hawarden, H.E. Matthews, E.I. Robson, A. Eckart. Astrophysical J., **565**, 131 (2002). DOI: 10.1086/324494

[6] S.W. Smye, J.M. Chamberlain, A.J. Fitzgerald, E. Berry. Phys. Med. Biol., **46**, R101 (2001).

[7] A.J. Huber, F. Keilmann, J. Wittborn, J. Aizpurua, R. Hillenbrand. Nano Lett., **8** (11), 3766 (2008). DOI: 10.1021/nl802086x

[8] A. Redo-Sanchez, B. Heshmat, A. Aghasi, S. Naqvi, M. Zhang, J. Romberg, R. Raskar. Nat. Commun., **7**, 12665 (2016). DOI: 10.1038/ncomms12665

[9] R. Piesiewicz, M. Jacob, M. Koch, J. Schoebel, T. Kürner. IEEE J. Selected Topics in Quant. Electron., **14** (2), 421 (2008). DOI: 10.1109/JSTQE.2007.910984

[10] R. Filip. Phys. Rev. A, **77**, 022310 (2008). DOI: 10.1103/PhysRevA.77.022310

[11] P. Papanastasiou, C. Ottaviani, S. Pirandola. Phys. Rev. A, **98**, 032314 (2018). DOI: 10.1103/PhysRevA.98.032314

[12] C. Ottaviani, M.J. Woolley, M. Erementchouk, J.F. Federici, P. Mazumder, S. Pirandola, C. Weedbrook. IEEE J. Selected Areas Commun., **38** (3), 483 (2020). DOI: 10.1109/JSAC.2020.2968973

[13] Z. Wang, R. Malaney, J. Green. Conference: ICC 2019 — 2019 IEEE Intern. Conf. Commun. (2019). DOI: 10.1109/ICC.2019.8761168

[14] Yu.V. Gulyaev, P.E. Zil'berman, E.M. Epshtein, R.J. Elliott. J. Commun. Technol. Electron., **48**, 942 (2003).

[15] A.M. Kadigrobov, Z. Ivanov, T.Claeson, R. Shekhter. Europhys. Lett., **67**, 948 (2004). DOI: 10.1209/epl/i2004-10159-8

[16] Yu.V. Gulyaev, P.E. Zilberman, A.I. Krikunov, A.I. Panas, E.M. Ephshtein. JETP Lett., **85**, 160 (2007). DOI: 10.1134/S002136400703006X

[17] Y.V. Gulyaev, P.E. Zilberman, I.V. Malikov, G.M. Mikhailov. JETP Lett., **93**, 259 (2011). DOI: 10.1134/S0021364011050055

[18] V. Korenivski, A. Iovan, A. Kadigrobov, R.I. Shekhter. Europhys. Lett., **104**, 27011 (2013). DOI: 10.1209/0295-5075/104/27011

[19] Yu.V. Gulyaev, P.E. Zilberman, A.I. Panas, E.M. Epstein, S.G. Chigarev. Patent RF № 2464683 (in Russian). Byul. № 29, 20.10.2012 (in Russian).

[20] E.A. Vilkov, Y.V. Gulyaev, P.E. Zilberman, A.I. Panas, S.G. Chigarev, I.V. Malikov, G.M. Mikhailov, A.V. Chernykh. Patent RF № 2688096 (in Russian). Byul. № 30, 20.05.2019 (in Russian).

[21] E.A. Vilkov, G.M. Mikhailov, S.G. Chigarev, Yu.V. Gulyaev, V.N. Korenivskii, S.A. Nikitov, A.N. Slavin. J. Commun. Technol. Electron., **61**, 995 (2016). DOI: 10.1134/S1064226916090138

[22] E.A. Vilkov, Yu.V. Gulyaev, P.E. Zil'berman, I.V. Malikov, G.M. Mikhailov, A.I. Panas, A.V. Chernykh, S.G. Chigarev. J. Commun. Technol. Electron., **60**, 1044 (2015). DOI: 10.1134/S1064226915090119

[23] P.A. Belov, R. Marque's, S.I. Maslovski, I.S. Nefedov, M. Silveirinha, C.R. Simovski, S.A. Tretyakov. Phys. Rev. B, **67**, 113103 (2003). DOI: 10.1103/ PhysRev.67.113103

[24] B.D.F. Casse, W.T. Lu, Y.J. Huang, E. Gultepe, L. Menon, S. Sridhara. Appl. Phys. Lett., **96**, 023114 (2010). DOI: 10.1063/1.3291677

[25] A. Tuniz, K.J. Kaltenecker, B.M. Fischer, M. Walther, S.C. Fleming, A. Argyros, B.T. Kuhlmey, Nature Commun., **4**, 2706 (2013). DOI: 10.1038/ncomms3706

[26] W. Ping, X. Wen, L. Longlong, Z. Chao. Rare Metal Mater. Engineer., **44** (12), 3014 (2015). DOI: 10.1016/s1875-5372(16)60041-3

[27] A.S. Shatalov, D.L. Zagorsky, S.G. Chigarev, I.N. Dyuzhikov. Patent №2715892. Byul. „Inventions. Poleznye Modeli ", 2020, №7. (in Russian).

[28] Y.V. Gulyaev, S.G. Chigarev, A.I. Panas, E.A. Vilkov, D.L. Zagorskiy, A.S. Shatalov. Tech. Phys. Lett., **45**, 271 (2019). DOI: 10.1134/S1063785019030271

[29] A.A. El-Saftawy, A. Elfalaky, M.S. Ragheb, S.G. Zakhary. Radiation Phys. Chem., **102**, 96 (2014). DOI: 10.1016/j.radphyschem.2014.04.025

[30] E.A. Vilkov, G.M. Mikhailov, S.A. Nikitov, A.R. Safin, M.V. Logunov, V.N. Korenivskii, S.G. Chigarev, L.A. Fomin. Phys. Solid State, **61** (6), 941 (2019). DOI: 10.1134/S1063783419060283

[31] E.A. Karashtin. JETP Lett., **112**, 122 (2020). DOI: 10.1134/S0021364020140106

[32] [Electronic source] Available at: https://math.nist.gov/ oommf/ Last updated: September 30, 2021.